

Unexpected Novel Binding Mode of Pyrrolidine-Based Aspartyl Protease Inhibitors: Design, Synthesis and Crystal Structure in Complex with HIV Protease

Edgar Specker,^[a] Jark Böttcher,^[a] Sascha Brass,^[a] Andreas Heine,^[a] Hauke Lilie,^[b] Andreas Schoop,^[c] Gerhard Müller,^[d] Nils Griebenow,^[e] and Gerhard Klebe^{*[a]}

At present nine FDA-approved HIV protease inhibitors have been launched to market, however rapid drug resistance arising under antiviral therapy calls upon novel concepts. Possible strategies are the development of ligands with less peptide-like character or the stabilization of a new and unexpected binding-competent conformation of the protein through a novel ligand-binding mode. Our rational design of pyrrolidinedimethylene diamines was inspired by the idea to incorporate key structural elements from classical peptidomimetics with a non-peptidic heterocyclic core comprising an endocyclic amino function to address the catalytic aspartic acid side chains of Asp25 and 25'. The basic scaffolds were decorated by side chains already optimized for the recognition pockets of HIV protease or cathepsin D. A multistep synthesis has been established to produce the central heterocycle and to give flexible access to side chain decorations. Depending on the substitution pattern of the pyrrolidine moiety, single-digit micromolar inhibition of HIV-1 protease and cathepsin D has been achieved. Successful design is suggested in agreement with our modelling concepts. The subsequently determined crystal

structure with HIV protease shows that the pyrrolidine moiety binds as expected to the pivotal position between both aspartic acid side chains. However, even though the inhibitors have been equipped symmetrically by polar acceptor groups to address the flap water molecule, it is repelled from the complex, and only one direct hydrogen bond is formed to the flap. A strong distortion of the flap region is detected, leading to a novel hydrogen bond which cross-links the flap loops. Furthermore, the inhibitor addresses only three of the four available recognition pockets. It achieves only an incomplete desolvation compared with the similarly decorated amprenavir. Taking these considerations into account it is surprising that the produced pyrrolidine derivatives achieve micromolar inhibition and it suggests extraordinary potency of the new compound class. Most likely, the protonated pyrrolidine moiety experiences strong enthalpic interactions with the enzyme through the formation of two salt bridges to the aspartic acid side chains. This might provide challenging opportunities to combat resistance of the rapidly mutating virus.

Introduction

Over nearly 20 years of aspartyl protease research, a plethora of inhibitors has been developed to prevent the catalytic activity of enzymes of this class.^[1] Most drug-development projects intended the design of peptidomimetics that substitute the substrate's peptide cleavage site by a suitable transition-state isostere.^[2] The first generation of such substrate analogue inhibitors failed as drug candidates due to limited oral bioavailability as a consequence of overly high molecular weight or overly pronounced reminiscence to an unfavourable peptidic character.^[3] Experience has shown that the success of such peptidomimetic concepts depends significantly on the aspartyl protease selected as drug target. For instance, the discovery of highly potent and orally available drugs for HIV protease was much easier and faster to accomplish compared with renin. This can be rationalized either historically or scientifically. Once the crystal structure of the HIV protease was solved in 1989 disclosing its membership to the aspartyl protease family, the entire experience and knowledge collected in former renin

projects fuelled the development of novel HIV protease inhibitors.^[4] Furthermore, in contrast to renin, HIV protease recognizes a much smaller peptide sequence through a limited

[a] Dr. E. Specker, J. Böttcher, S. Brass, Dr. A. Heine, Prof. G. Klebe
Institut für Pharmazeutische Chemie
Philipps-Universität Marburg
Marbacher Weg 6, 35032 Marburg (Germany)
Fax: (+49) 6421-282-8994
E-mail: klebe@mail.uni-marburg.de

[b] Dr. H. Lilie
Institut für Biotechnologie
Martin-Luther-Universität Halle-Wittenberg
Kurt-Mothes-Straße 3, 06120 Halle (Saale) (Germany)

[c] Dr. A. Schoop
Boehringer Ingelheim, Wien (Austria)

[d] Dr. G. Müller
GPC Biotech, München (Germany)

[e] Dr. N. Griebenow
Bayer AG, Elberfeld (Germany)

number of tightly binding specificity pockets on both sides of the cleavage site. This fact provided the opportunity to design inhibitors of lower molecular weight and accordingly, more favourable pharmacokinetic properties.^[5] Although at present nine FDA-approved HIV protease inhibitors have been successfully launched to market, the research for novel inhibitors has not, and most likely will not, come to a final conclusion.^[6,7] This is mainly due to the fact that rapid drug resistance arises under antiviral therapy caused by insufficient suppression of the fast and error-prone replication rate of the HIV virus.^[8] One concept to break drug resistance has been suggested through the development of ligands with less peptide-like character. This strategy has been successfully achieved with the novel HIV protease inhibitor tipranavir (**1**, Figure 1).^[9] An alternative idea is aimed at stabilizing a novel unexpected binding-com-

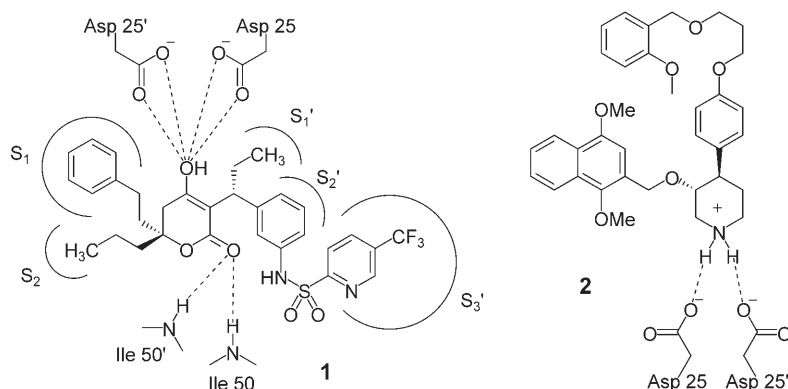


Figure 1. Structures of tipranavir (**1**), an HIV-1 protease inhibitor (IC_{50} = 30 nM) and the piperidine derivative **2**, a renin inhibitor (IC_{50} = 0.06 nM). In each case, binding-site interactions are highlighted.

petent conformation of the protein or selecting a new ligand binding mode. The latter has been successfully accomplished by the piperidine-type inhibitor **2**, discovered by Roche as potent renin inhibitor (Figure 1).^[10,11] Furthermore, elaborated thermodynamic studies performed by Freire et al.^[12] have demonstrated that the virus less readily escapes inhibitors through successful mutagenesis if the binding of the inhibitors is pronouncedly enthalpy-driven. In consequence, it appears advisable to equip novel types of HIV inhibitors by as many pronounced enthalpic interaction features as possible.

Tipranavir (**1**) was described in 1999 by Thaisrivongs and Strohbach as a novel, potent, orally bioavailable heterocyclic HIV protease inhibitor with activity against selected mutants.^[9] It addresses, similarly to a peptide substrate, the subpockets S_2 to S_3' , and accordingly it comprises five different side chains P_2 to P_3' and gains an additional entropic contribution by replacing the structural water molecule ("flap water") in the HIV protease binding pocket. The carbonyl function of the heterocyclic 5,6-dihydropyran-2-one moiety interacts directly via hydrogen bonds with the backbone NH groups of Ile50 and 50' in the flap loops. A precursor of **2** showing a similar piperidine moiety was discovered as a screening hit by Hoffmann-La

Roche.^[10,11] In the following, these substituted piperidines were developed as a new structural entity for renin inhibitors bearing as a key element the most likely protonated endocyclic amine. It occupies the pivotal position between both catalytic aspartic acid side chains, thus forming two enthalpically favourable ionic hydrogen bonds. In addition, **2** stabilizes renin in a conformation previously not yet observed and accommodates the inhibitor in a novel unexpected binding mode. However, this new binding-competent enzyme conformation is well in agreement with opportunistic conformational transitions required for the flap opening to give the substrate access to the active site. Very recently a novel structure has been reported on a plasmepsin-II complex exhibiting a very similar enzyme conformation with open flap geometry.^[13] Interestingly enough, this inhibitor does not form a direct interaction to

both aspartate groups through one of its functional groups. Instead, such a contact is mediated through an active site water molecule trapped between the inhibitor and catalytic aspartic acid side chains at the likely position of the water taking the role of the nucleophile during the enzymatic cleavage reaction.

Our rational design of pyrrolidinedimethylene diamines described herein was inspired by the idea to incorporate key structural elements from classical peptidomimetics with a non-peptidic heterocyclic core structure comprising an endocyclic amino function to address the catalytic aspartic acid side chains. Figure 2 illustrates schematically the structural consideration for the design of our novel prototype inhibitors. The concept departs from the crystal structures of HIV protease and cathepsin D with the bound peptidomimetic pepstatin (**3**). The hydroxy group of the latter, incorporated into a statine moiety, interacts through hydrogen bonds with both catalytic aspartic acid side chains. Furthermore, important hydrogen bonds are formed by both amide carbonyl groups on either side of the cleavage site. They interact through the flap water molecule in the active site of HIV protease with the NH groups of Ile50 and Ile50' or directly with the nitrogen atoms of Gly79 and Asp80 of the cathepsin D backbone.^[14,15] To assess whether the pyrrolidinedimethylene diamines exhibit a valid new lead structure, the central pyrrolidine core was decorated by already optimized side chains derived from the HIV protease inhibitor amprenavir (**4**) and cathepsin D inhibitor **5**.^[16,17]

In summary, the pyrrolidinedimethylene diamines were designed to fulfil the following five requirements:

1. an endocyclic amine such as pyrrolidine with a protonated nitrogen atom, which addresses the two catalytic aspartic acid side chains;
2. two carbonyl or sulfone groups as hydrogen-bond acceptors to form hydrogen bonds either to the flap water molecule (HIV protease) or the NH groups of Gly79 and Asp80 of the cathepsin D backbone;

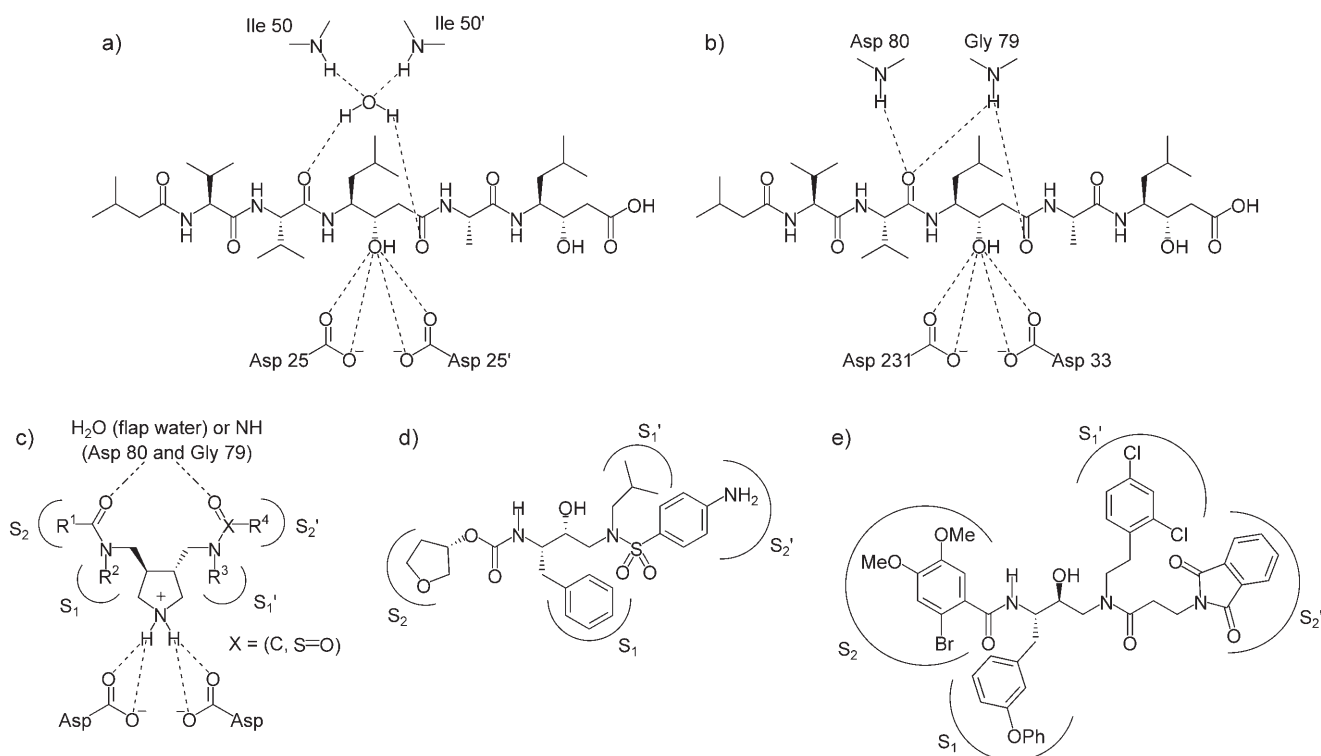
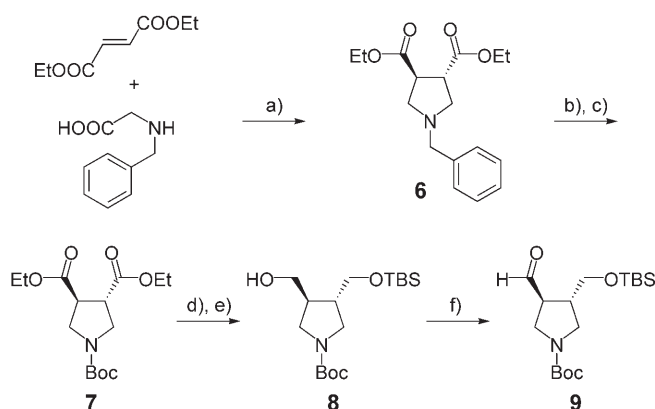


Figure 2. Rational design strategy leading to pyrrolidinedimethylene diamines: a) hydrogen bonds of pepstatin (**3**) in the active site of HIV-1 protease; b) hydrogen bonds of pepstatin (**3**) in the active site of cathepsin D; c) general pyrrolidinedimethylene diamine structure; d) HIV-1 protease inhibitor amprenavir ($K_i = 0.6 \text{ nM}$); e) cathepsin D inhibitor **5** ($K_i = 0.7 \text{ nM}$).

3. decoration of the pyrrolidine core with four already established side chain decorations P_2 – P_2' accommodating the S_2 – S_2' pockets of each protease;
4. linkage between P_2 – P_1 and P_1' – P_2' fragments by amide or sulfonamide bonds;
5. stereochemical *trans* configuration at the pyrrolidine core moiety to achieve an orientation of the P_2 , P_1 and P_1' , P_2' decorations analogous to the peptide backbone conformation of pepstatin.



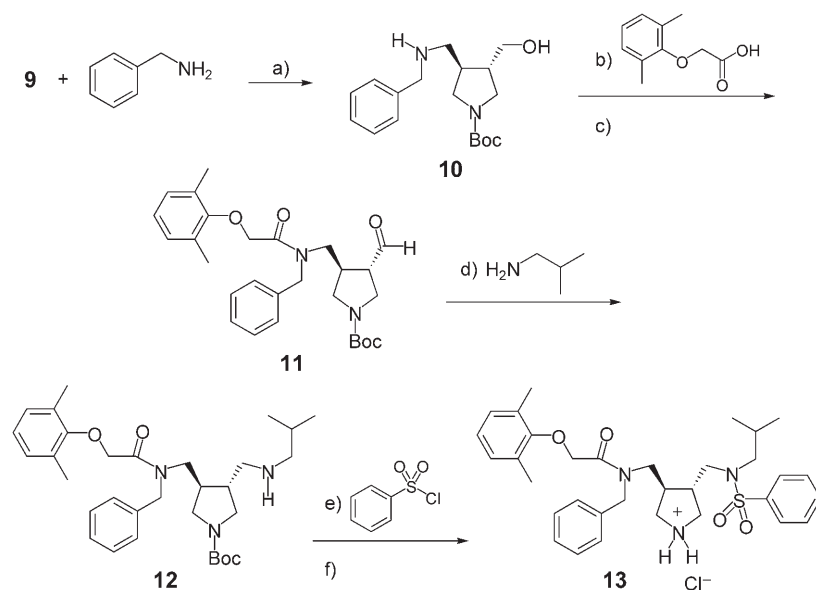
Scheme 1. Synthesis of aldehyde **9** as initial building block: a) $(\text{CH}_2\text{O})_n$, 78%; b) H_2 , Pd/C, 98%; c) TEA, Boc_2O , 95%; d) LiBH_4 , THF, 84%; e) imidazole, TBSCl, 90%; f) $(\text{COCl})_2$, DMSO, DIPEA, 98%. Boc = *tert*-butoxycarbonyl, DIPEA = *N,N*-diisopropylethylamine, TBSCl = *tert*-butyldimethylsilyl chloride, TEA = triethylamine.

Results and Discussion

Chemical synthesis

Scheme 1 illustrates the synthesis of aldehyde **9**. Reaction of *N*-benzylglycine with paraformaldehyde resulted in the formation of an azomethine ylide as dienophile, which was converted with diethyl fumarate as the dipolarophile in a 1,3-dipolar cycloaddition into the pyrrolidine core structure. Decarboxylation provided **6** as pyrrolidine scaffold, exhibiting *trans*-substituted diethylester functions. Reductive cleavage of the benzyl group furnished a free amino function, which was protected with a Boc group to **7**. Reduction of the diethylester with LiBH_4 afforded a diol which was converted into **8** by protection of only one alcohol group with TBSCl. Swern oxidation revealed the aldehyde **9**.^[18]

Scheme 2 describes the decoration of the pyrrolidine scaffold to produce **13**. Synthesis commenced with a reductive amination of **9** using benzylamine and $\text{Me}_3\text{NBH}(\text{OAc})_3$ followed by acid extraction with 1 *N* HCl that resulted in the deprotection of the alcohol function to form **10**.^[19] Coupling with 2,6-dimethylphenoxycarboxylic acid and subsequent Swern oxidation of the alcohol accomplished **11**.^[18] After reductive amination with isobutylamine as described above, **12** was coupled with benzenesulfonyl chloride. Deprotection with HCl/dioxane



Scheme 2. Functionalization of the pyrrolidine core with residues optimized for HIV-1 protease: a) $(\text{OAc})_3\text{BHNMe}_4$, HCl (1 N), 75%; b) with EDC, HOBT; c) $(\text{COCl})_2$, DMSO, DIPA, 68% for steps b) and c); d) with $(\text{OAc})_3\text{BHNMe}_4$, 75%; e) with TEA; f) HCl (4 N) in dioxane, 85% for steps e) and f). DIPA = diisopropylamine, EDC = 3-(3-dimethylamino-propyl)-1-ethylcarbodiimide, HOBT = 1-hydroxy-1H-benzotriazole.

yielded the pyrrolidinedimethylene diamine **13** as final product. The very similar synthesis of **16–17**, starting from the pyrrolidine scaffold **10**, will be described explicitly elsewhere.^[20]

Biological evaluation

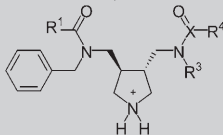
Racemic mixtures of compounds **13–17** were tested against HIV protease. Inhibition constants were determined using a standard assay.^[21,22] The initial rate of enzymatic cleavage of the synthetic fluorophore-labelled substrates Abz-Thr-Ile-Nle-(*p*-nitro)-Phe-Gln-Arg-NH₂ for HIV protease and (MOCac)-GKPILFFRLK-(Dnp)-NH₂ for cathepsin D was measured in the presence of varying concentrations of inhibitors **13–17** (see Materials and Methods). IC₅₀ values are given in Table 1.

All compounds in the series were decorated by an *N*-benzyl moiety (R^2) planned to address the S_1 subsite. Variations were achieved in all remaining positions. Clearly single-digit micromolar inhibition is achieved against HIV protease once a sulfonamide group is present, whereas higher-affinity binding

towards cathepsin D is experienced if both H-bond acceptor sites are formed by amide functions. In the series **13–15**, attachment of a *p*-amino group on R^4 results in nearly identical binding affinity compared with the unsubstituted derivative. Expansion of the phenyl moiety by a hydrophobic methyl group in the *para* position parallels a loss in affinity by one order of magnitude. Supposedly, a similar spatial restriction of the accommodated subsite in HIV protease is also experienced by **16** and **17** with sterically bulkier R^4 groups. For cathepsin D, R^4 groups of increasing steric demand appear beneficial for binding. Furthermore, the subsite addressed by the R^3 substituent seems to be larger in cathepsin D compared with HIV protease, as higher affinity is achieved by the ligand exhibit-

ing a dichlorophenethyl portion at this position compared with an isobutyl group in **13–15**, which show more potency towards HIV protease. The deviating substituents R^1 selected as optimally suited for either HIV protease or cathepsin D are

Table 1. Inhibition of HIV-1 protease and cathepsin D by compounds **13–17**.

						
Compd	R^1	R^3	R^4	X	HIV-1 protease IC ₅₀ [μM]	Cathepsin D IC ₅₀ [μM]
13				S=O	2.2	> 40
14				S=O	3.3	> 40
15				S=O	12.1	> 40
16				C	19.8	1.05
17				C	22.1	0.57

of similar steric bulk; however, the portion better suited for cathepsin D has been decorated by bromine and two methoxy groups. Clearly, the site in cathepsin D hosting the R¹ substituent is of slightly higher polar character.

A more conclusive discussion of the indicated structure–activity relationship requires further details about the adopted binding modes of **13–17** in both target enzymes.

Modelling studies

To obtain a first insight into the putatively adopted binding mode at the active site of HIV protease, docking was performed with AutoDock.^[23,24] As potential fields in AutoDock, knowledge-based potentials from DrugScore were used.^[25,26] As reference coordinates for docking, the crystal structure of HIV protease with bound amprenavir (PDB code: 1HPV) was considered.^[16]

As the first target compound, both enantiomers of the best binding inhibitor **13** were selected and docked into the crystal structure of the HIV protease–amprenavir complex. In our docking study, we considered the structural water next to the flap and anticipated that it would mediate hydrogen bonds to both Ile50NH groups in the flap. For both enantiomers, a binding mode placing the pyrrolidine nitrogen atom well between both aspartate groups was suggested. Furthermore, occupation of the subsites P₂, P₁, P₁', and P₂' in a manner similar to that of amprenavir could be achieved. However, only the amide carbonyl group was involved in hydrogen-bond formation to Ile50NH, whereas the SO₂ group remained unsatisfied. Overall, a rather crowded arrangement next to the catalytic centre was noticed. With respect to both enantiomers, docking of (*S,S*)-**13** achieved the better scoring with DrugScore; for the inverted (*R,R*) stereoisomer, the solution suggested by docking received a lower score.

Crystal structure analysis

Subsequent to our modelling study, we successfully obtained well-diffracting crystals with bound **13**. They were grown from a solution in the presence of a racemic mixture of the inhibitor. Data collection details and refinement statistics are given in Table 2. With respect to our initial design concept and in agreement with our docking attempts, the central pyrrolidine moiety is found at the pivotal position between both catalytic aspartate groups (Figure 3). As expected, the endocyclic amino group of the pyrrolidine is a perfect substitute for the hydroxy group in the classical transition-state analogues. However, apart from this successful prediction, significant deviations from our proposed docking modes are observed in the experimentally determined structure.

Instead of the predicted *S,S* enantiomer, (*R,R*)-**13** is bound to the protein. The design concept was aimed at decorating the central skeleton with side chains already optimized for other well-established HIV protease inhibitors such as amprenavir. However, the determined binding mode does not show this anticipated correspondence. Most important, the structural flap water is replaced from the complex, and the inhibitor

Table 2. Data collection and refinement statistics of the (*R,R*)-**13**–HIV-1 protease crystal structure.

Feature	Data
resolution [Å]	20–1.5
space group	<i>P</i> ₂ ₁ ₂ ₁ ₂ ₁
	<i>a</i> = 51.9
cell dimensions [Å]	<i>b</i> = 57.7
	<i>c</i> = 62.2
highest resolution shell [Å]	1.53–1.5
no. measured reflections	109 029
no. independent reflections	29 849
completeness [%]	97.5 [77.3] ^[a]
<i>I</i> / <i>σ</i>	18.6 [1.6] ^[a]
<i>R</i> _{sym} [%]	6.3 [54.0] ^[a]
refined residues	198
refined ligand atoms	41
refined water molecules	190
refined glycerol molecules	2
refined Cl atoms	2
resolution in refinement [Å]	8–1.5
<i>R</i> _{cryst} (<i>F</i> > 4 <i>σ F</i> _o ; <i>F</i> _o)	16.7; 18.1
<i>R</i> _{free} (<i>F</i> > 4 <i>σ F</i> _o ; <i>F</i> _o)	22.0; 23.6
mean B-factor [Å ²]	16.7 (chain A)
	19.0 (chain B)
main chain [Å ²]	13.1 (chain A)
	15.8 (chain B)
side chains [Å ²]	20.6 (chain A)
	22.5 (chain B)
ligand [Å ²]	33.0
water [Å ²]	29.0
glycerol [Å ²]	52.8
Cl ions [Å ²]	20.2
Ramachandran plot:	
most favored geometry [%]	94.9
additionally allowed [%]	5.1
generously allowed [%]	0
disallowed [%]	0

[a] Values in square brackets refer to the shell of highest resolution.

forms a direct hydrogen bond to the backbone NH group of Ile50 through one of its sulfoxo oxygen atoms (Figure 3). The second acceptor functionality, the carbonyl oxygen atom of the amide group, introduced into the ligand to serve as second binding partner to the flap water, remains unsatisfied without forming any further polar contacts to the enzyme. Possibly provoked by the lack of a suitable hydrogen-bonding partner of the ligand and assisted by some sterically induced conformational distortions, the NH backbone functionality of Ile50' forms a hydrogen-bonding contact to the carbonyl group of the amide bond of Ile50. This additional connection across both flap loops supposedly stabilizes the dimer in the flap region (Figure 3 and 6). It serves as a sort of surrogate for the abandoned contact originally formed through the bridging structural water molecule, which is no longer observed in the complex with (*R,R*)-**13**. This unusual geometry of the flap parallels a significant distortion (up to 4.9 Å) of the polymer chain compared, for example, with the complex formed with amprenavir. As mentioned, the anticipated decoration of **13** did not result in the expected occupancy of the specificity pockets S₂, S₁, S₁', and S₂'. Compared with amprenavir, an overall rotated arrangement of the inhibitor is observed (Figure 4). An approx-

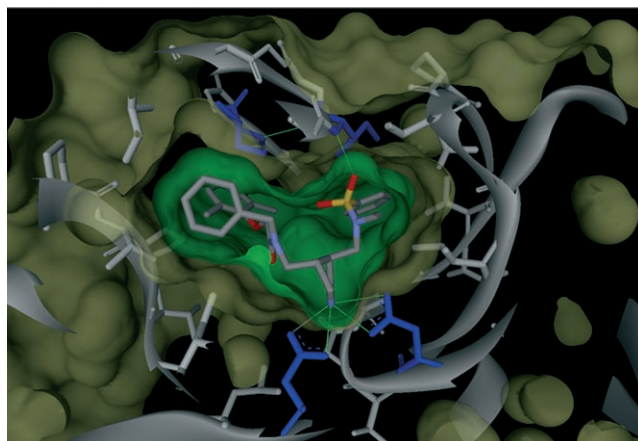


Figure 3. (*R,R*)-**13** (shown with solvent accessible surface, green) binds with its central pyrrolidine moiety at the pivotal position between both catalytic aspartate groups Asp25 and 25' (blue) of the protease (grey, yellow surface). It is a perfect substitute for the hydroxy group in the classical transition-state analogues. The structural flap water molecule is expelled from the complex and (*R,R*)-**13** forms a direct hydrogen bond to the backbone NH group of Ile50 (blue) through one of the sulfoxy oxygen atoms. The second acceptor functionality, the carbonyl oxygen atom of the amide group, originally introduced to serve as second H-bonding group for the flap region, remains unbound without forming any further polar contacts to the enzyme. As a consequence of the sterically induced conformational distortions of the flap, the NH backbone functionality of Ile50' forms a hydrogen-bonding contact to the carbonyl group of the amide bond of Ile50.

imate correspondence in the occupation of S_1 and S_2' can be assigned with respect to the isobutyl group of **13** and the benzyl moiety of amprenavir in S_1 , and the phenyl sulfonamide substituents of both inhibitors hosted in S_2' . The remaining two decorations of **13**, the *N*-benzyl and dimethylphenoxy group are clustered together and occupy the S_1' pocket, suggesting a sort of overcrowding (Figure 4, 5). The dimethylphenoxy group penetrates into the bordering solvent environment. As it approaches the flap loop rather closely, it possibly perturbs its orientation (Figure 6). Interestingly enough, the S_2 pocket remains virtually unoccupied; the *N*-benzyl substituent of **13** only slightly penetrates into this subsite (Figure 4, 5).

Directly facing the ligand surface portions that get buried upon complex formation reveals a 95% burial for amprenavir, whereas **13** is only at 85% in surface contact with the enzyme (Figure 5, 6). The complexes with amprenavir and **13** crystallize in different space groups. However, structural comparison with other complexes found in either space groups does not indicate any correlations between distortions of the flap region and crystal packing. Thus, it appears rather unlikely that the crystallographic environment has a significant impact on the flap perturbations observed in **13**. Accordingly, it can be assumed that the unexpected and distorted binding mode is clearly induced by the properties of the bound ligand. In this context it is of interest whether similar distortions have already been observed in any other HIV protease complexes. To perform such analysis across a representative data set of complexes, we applied Cavbase, a new approach developed in our laboratory, to compare binding pockets.^[27,28] Cavbase mutually faces binding pockets in terms of matching physicochemical

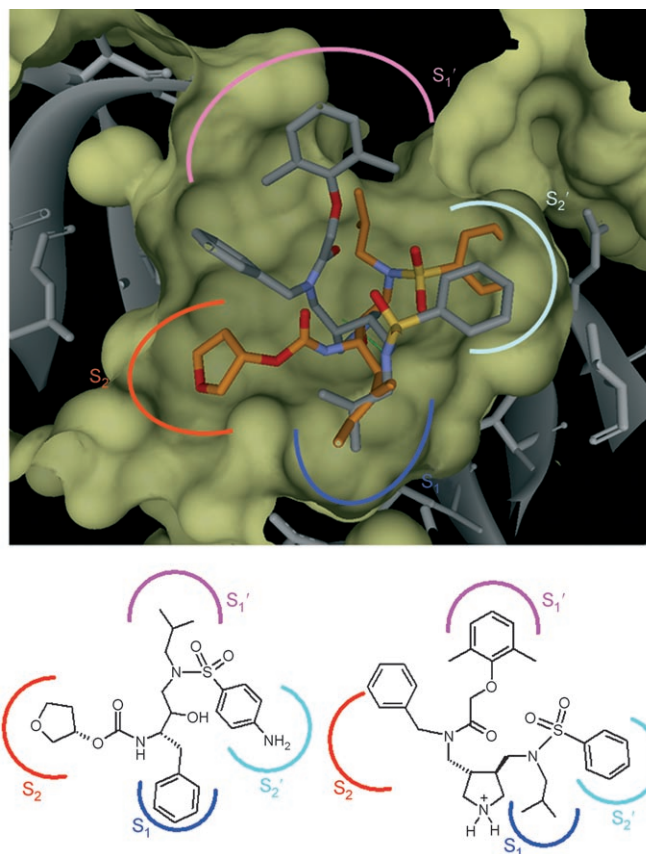


Figure 4. Compared with amprenavir, (*R,R*)-**13** adopts a deviating binding mode resulting in a different occupation of the four specificity pockets S_2' , S_1 , S_1' , and S_2 . An approximate correspondence in occupation of S_1 and S_2' can be assigned to the isobutyl group of **13** and the benzyl moiety of **4** in S_1 , and the phenyl sulfonamide substituents of both inhibitors hosted in S_2' . The remaining two decorations of **13**, the *N*-benzyl and dimethylphenoxy group are clustered together and occupy the S_1' pocket, suggesting a sort of overcrowding (Figure 4, 5). The dimethylphenoxy group penetrates into the bordering solvent environment. As it approaches the flap loop rather closely, it possibly perturbs its orientation (Figure 6). Interestingly enough, the S_2 pocket remains virtually unoccupied; the *N*-benzyl substituent of **13** only slightly penetrates into this subsite (Figure 4, 5).

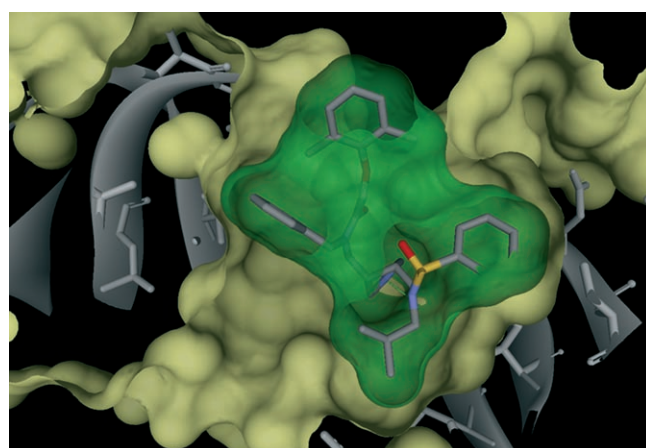


Figure 5. Binding mode of **13** shown together with solvent accessible surface (protein, yellow; **13**, green). The bulky terminal 2,6-dimethylphenoxy group exceeds beyond the S_1' binding pocket into the adjacent solvent environment.

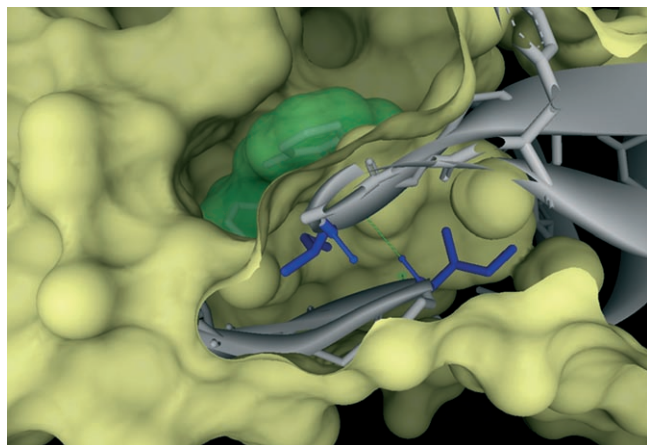


Figure 6. The bulky 2,6-dimethylphenoxy group of **13** penetrates into the S_1' pocket and the adjacent solvent environment, simultaneously pushing one of the flap regions into a distorted conformation. The inhibitor forms one direct hydrogen bond to the backbone NH group of Ile 50 (blue, left) whereas the peptide bond to Ile 50' (blue, right) is rotated and forms a hydrogen bond (green) to the neighbouring flap loop.

properties exposed to the cavity surface. The idea of this approach is that protein function is intimately connected with the recognition of endogenous ligands in well-characterized clefts or cavities on the protein surface. Accordingly, similar function requires similarity in the shape of such binding pockets. The amino acids flanking the cavities are reduced to a set of generic pseudocenters representing their recognition properties. Furthermore their surface exposure is examined and the surface patches that fall next to each pseudocenter under consideration are used in the comparison as descriptors of the shape of the cavities. A mutual cavity similarity is discovered using a clique detection algorithm that searches for maximal sub-graph matching of exposed pseudocenters. Finally, multiple solutions from this sub-graph matching are scored in terms of commonly exposed surface patches corresponding to equivalent physicochemical properties.

We applied this approach by taking the binding pocket of HIV protease in complex with **13** as a reference, and screened this binding pocket against a set of 135 cavities extracted from crystal structures of HIV protease complexes deposited in the Protein Data Bank. In Table 3 the 10 most similar pockets with respect to **13** are listed. As most similar to our decoy pocket, an example with a bound ligand of the cyclic urea-type has been matched. The latter inhibitor repels the flap water molecule in a manner similar to **13**. However, the complex formed does not exhibit similar flap distortions. Supposedly, the described complex with **13** represents a novel binding mode which leaves one binding pocket unoccupied and provokes a distortion of the flap loops previously not yet observed to a similar extent.

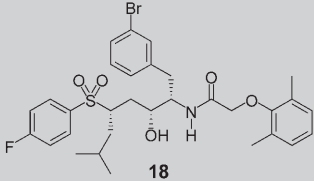
For comparison we selected the binding pocket of HIV protease in complex with the hydroxyethylene sulfone-based inhibitor **18** (Table 4) for which we recently determined the crystal structure.^[29] This inhibitor binds to the enzyme without pronounced distortions, and its interactions are mediated through

Table 3. The 10 binding pockets in HIV-1 protease complexes scored by Cavbase as most similar with the binding pocket in the complex with **13**.

PDB Code	Score	No. Corresponding Pseudocenters	RMS Deviations [Å]
1AJX ^[36]	36.44	41	0.59
1K6C ^[37]	36.33	40	0.88
1CPJ ^[38]	36.31	40	0.50
1K6T ^[37]	35.77	40	0.66
1HSG ^[39]	35.75	41	0.78
1K6P ^[37]	35.59	40	0.72
1YTH ^[40]	35.53	39	0.44
1MTR ^[41]	35.48	39	0.74
1DAZ ^[42]	35.42	39	0.54
1YTG ^[40]	35.04	39	0.51

the flap water molecule to the protein. Taking the pocket of this complex as a probe cavity for our search against the 135 HIV protease entries with Cavbase revealed the complexes listed in Table 4 as the most similar examples. With respect to

Table 4. The 10 binding pockets in HIV-1 protease complexes scored by Cavbase as most similar with the binding pocket in the complex with **18**.

 18			
PDB Code	Score	No. Corresponding Pseudocenters	RMS Deviations [Å]
1HSG ^[39]	53.26	56	0.51
1G35 ^[43]	51.84	55	0.43
4PHV ^[44]	49.41	53	0.51
1FFI ^[45]	48.83	52	0.52
2BPY ^[46]	48.76	53	0.52
4HVP ^[47]	48.72	53	0.60
2BPZ ^[46]	48.50	53	0.53
1FG6 ^[45]	48.43	51	0.41
1HVJ ^[48]	48.06	52	0.60
1FEJ ^[45]	47.41	51	0.49

the pocket of **18**, significantly better similarity scores are calculated and a higher portion of corresponding pseudocenters are matched compared with the cavity extracted from the complex with **13**. This fact clearly indicates that the geometry of the complex with **18** is by far better in accordance with the usually detected architecture found for HIV protease inhibitor complexes.

Conclusions

A novel skeleton to address the pivotal position between the catalytic dyad of aspartyl proteases has been designed and incorporated into potent inhibitors. The central building block is

formed by a pyrrolidine moiety which has been decorated by side chains transferred from other ligands known as potent inhibitors of this protein family. A multistep synthesis has been developed and conceived in a way to give flexible access to multiple decorations. Determination of the inhibitory potency of individual members of the series reveals single-digit micromolar binding to HIV protease or cathepsin D. So far, successful design is suggested and agreement with the modelling concept appears to be given. However, this view has to be revised to some extent, consulting the subsequently determined crystal structure with HIV protease. The pyrrolidine moiety binds as expected, proving this portion as a novel privileged scaffold to address the family of aspartyl proteases. Although the inhibitor has been equipped symmetrically by polar acceptor groups to address the flap water molecule, this group is repelled from the complex, and only one direct hydrogen bond is formed to the flap loop. A strong and obviously not yet observed distortion of the flap region is detected which leads to a novel cross-linking hydrogen bond that fixes both flap loops. Furthermore, the inhibitor addresses only three of the four available binding pockets and achieves only an incomplete desolvation compared with the similarly decorated amprenavir. It has to be admitted that the binding mode found by crystallography was unexpected; nevertheless, a novel potent class of inhibitors has been discovered. In our initial docking attempts, we failed to predict the correct binding mode and we initially picked the wrong stereoisomer as the more potent. However, in this analysis we did not consider the possibility of repelling the water from the binding site nor any strong distortions of the flaps. Retrospectively, under these assumptions, we cannot expect that the docking could have suggested the correct binding mode. Nevertheless, this unexpected result points to cautious ligand design and also underlines the value of crystallography in the drug discovery process. Without the latter method, the false assumptions would have never been detected. Most likely further design and synthesis would have converged after an elaborate and tedious structure–activity relationship in some non-conclusive correlations, indicating the unexpected binding mode. This clearly points either to some inherent limitations in design and modelling but equally well to the necessity to involve crystallography early on in drug discovery projects.

The detected binding mode of **13** does not suggest optimal ligand accommodation. The observed flap loop distortions appear costly. The incomplete desolvation of the ligand is most likely detrimental to high-affinity binding. Furthermore, the inhibitor leaves one subsite virtually unoccupied. Experience shows that such mismatch is rather expensive in terms of binding affinity. Taking these considerations together it appears surprising that **13** still achieves micromolar inhibition and suggests the extraordinary potency of the new compound class. Most likely, the protonated pyrrolidine moiety experiences strong enthalpic interactions with the enzyme through the formation of two salt bridges to the aspartic acid side chains. This might provide challenging opportunities to combat resistance of the rapidly mutating virus. As indicated by recent thermodynamic studies of Freire and co-workers, inhibitors binding

in an enthalpy-driven manner to the protease achieve improved resistance profiles compared with entropically favoured binders.^[12] Possibly this enthalpic advantage can be exploited systematically by correctly substituted pyrrolidines.

Experimental Section

Kinetic assays: Binding constants for inhibition of HIV protease were determined as previously described.^[21] IC_{50} values were taken from plots of V_i/V_0 versus inhibitor concentration, in which V_i is the velocity in presence, and V_0 the velocity in the absence of an inhibitor. The fluorogenic substrate Abz-Thr-Ile-Nle-(*p*-nitro)-Phe-Gln-Arg-NH₂ was purchased from Bachem. Recombinant HIV-1 protease was expressed from *Escherichia coli* and purified as previously described.^[30] Enzymatic assays were performed in 402.2 μ L assay buffer (100 mM MES, 300 mM KCl, 5 mM EDTA, 1 mg mL⁻¹ BSA, pH 5.5) by the addition of substrate dissolved in 8.4 μ L DMSO, distinct inhibitor concentrations dissolved in 8.4 μ L DMSO and 1 μ L HIV-1 protease to a final volume of 420 μ L (final DMSO concentration 4%). The hydrolysis of the substrate was recorded as the increase in fluorescence intensity (excitation wavelength 337 nm, emission wavelength 410 nm) over a time period of 10 min, during which the signal increased linearly with time.

The cathepsin D assay was measured using a fluorogenic peptide substrate (MOCAC)-GKPIFFRLK(Dnp)-NH₂ which contains a (7-methoxycoumarin-4-yl)acetyl group (MOCAC) as a fluorophore and a lysine-bound *N*'-(2,4-dinitrophenyl) group (Dnp) as a quencher in the same molecule. The fluorescent signal in the uncleaved substrate is quenched due to fluorescence resonance energy transfer (FRET) between fluorophore and quencher groups.^[22] The activity of cathepsin D (10 ng mL⁻¹) can be continuously monitored by the increase in fluorescence during substrate cleavage. The assay was performed in 100 μ L assay buffer (40 mM NaAc solution, 0.01 % Brij35, pH 4.0) by the addition of 12.5 μ M substrate and distinct inhibitor concentrations using Opti-plates 96. The hydrolysis of the substrate was recorded as the increase in fluorescence intensity (excitation wavelength 320 nm, emission wavelength 405 nm) over a time period of 25 min.

Crystallisation and structure determination: The HIV protease (7 mg mL⁻¹) in complex with the pyrrolidinemethylene diamine **13** crystallizes at 18 °C in 3 M NaCl, 0.1 M BisTris, pH 6.5 in space group $P2_12_12_1$ (crystal data, Table 2). The crystals were obtained by co-crystallization of the enzyme with the inhibitor at 1.9 mmol L⁻¹. For cryoprotection the crystals were briefly soaked in mother liquor containing 20% glycerol. The data set was collected at the synchrotron BESSY II in Berlin on PSF beamline I equipped with a MAR-CCD detector. 100 frames with $\delta\phi = 0.5^\circ$ at a crystal to detector distance of 100 mm were collected at -170 °C. Data were processed and scaled with Denzo and Scalepack.^[31] The structure was determined by the molecular replacement method implemented in AmoRe.^[32] The 1.85 Å structure of HIV-1 protease in complex with a macrocyclic inhibitor (PDB code: 1B6N)^[33] was used as a search model. Refinement was continued using SHELXL-97;^[34] for each

refinement step at least 10 cycles of conjugate gradient minimisation were performed, with restraints on bond distances, angles, and B-values. Intermittent cycles of model building were done with the program O.^[35] The coordinates have been deposited in the PDB (<http://www.rcsb.org/pdb/>) with access code 1XL2.

Spectroscopy and Analytics: ¹H and ¹³C NMR spectra were recorded on a Jeol Eclipse +500 MHz instrument, using [D₆]DMSO or CDCl₃ as solvents with TMS as internal standard. Chemical shifts are given in ppm (δ scale). Reactions were monitored by thin-layer chromatography (TLC) on precoated Alugram SIL G/UV plates from Macherey–Nagel, and spots were visualized with UV light (254 nm) or coloured with a solution of 6 g molybdotetraphosphoric acid, 2.5 g cer(IV)sulfate, 470 mL water, 30 mL concentrated H₂SO₄. Flash column chromatography was performed using silica gel (particle size 0.040–0.063 mm) supplied by Merck. THF was freshly distilled from LiAlH₄ under argon. Triethylamine, *N,N*-dimethylformamide (DMF), and dichloromethane were purchased from Aldrich and used without further purification. High resolution mass spectra (HRMS: EI and ESI) were performed with either a Micromass 7070 H or Micromass Autospec spectrometer. Elemental analyses were performed on a Charmomat 5-ADG from Wösthoff or HP-185. The HIV-1 protease assay was performed on a RF-5301 PC spectrofluorophotometer from Shimadzu and the cathepsin D assay was measured on a POLARstar spectrofluorophotometer from BMGLabtech.

Synthesis:

rac-(3*S*,4*S*)-(1-Benzyl-pyrrolidine-3,4-dicarboxylic acid diethylester (**6**): *N*-Benzyl-glycine (150 g, 907 mmol), diethyl fumarate (159.5 g, 926 mmol), and paraformaldehyde (32.7 g, 1.1 mol) were suspended in 1.3 L toluene and heated at reflux with a Dean–Stark trap. After 1 h the solution was filtered, concentrated in vacuo, and then distilled at 159 °C (0.9 mbar) to give **6** (214 g, 702 mmol, 78%) as a colorless oil. ¹H NMR (500 MHz, CDCl₃): δ = 1.23 (t, *J* = 7.2 Hz, 6H), 2.79 (dd, *J* = 9.3, 6.1 Hz, 2H), 2.89 (dd, *J* = 8.5, *J* = 7.8, 2H), 3.44 (m, 2H), 3.59 (s, 2H), 4.13 (d, *J* = 7.0 Hz, 4H), 7.25 ppm (m, 5H). ¹³C NMR (125 MHz, CDCl₃): δ = 14.1, 45.4, 56.5, 59.2, 60.8, 126.9, 128.1, 128.3, 138.3, 173.3 ppm. HRMS (EI) *m/z* C₁₇H₂₃NO₄ [MH⁺] calcd.: 305.1627; found: 305.1625. Anal. calcd. for C₁₇H₂₃NO₄: C 66.86, H 7.59, N 4.59; found: C 67.16, H 7.45, N 4.77.

rac-(3*S*,4*S*)-(Pyrrolidine-3,4-carboxylic acid diethylester: To a stirring solution of **6** (5.8 g, 19 mmol) in 20 mL THF containing Pd/C (10%, 322 mg) H₂ was bubbled (1 atm) at room temperature for 5 h. The reaction mixture was filtered through celite and concentrated in vacuo to give 4.01 g (98%) as a colorless oil. ¹H NMR (500 MHz, CDCl₃): δ = 1.26 (t, *J* = 7.1 Hz, 6H), 2.14 (m, 1H), 3.01 (m, 2H), 3.28 (m, 4H), 4.17 ppm (d, 4H, *J* = 7.1 Hz). ¹³C NMR (125 MHz, CDCl₃): δ = 14.5, 48.4, 52.2, 70.0, 173.9 ppm. HRMS (EI) *m/z* C₁₀H₁₇NO₄ [MH⁺] calcd.: 215.1153; found: 215.1158.

rac-(3*S*,4*S*)-Pyrrolidine-1,3,4-tricarboxylic acid 1-*tert*-butyl ester 3,4-diethyl ester (**7**): Boc₂O (3.77 g, 17.3 mmol) dissolved in 50 mL dioxane was added in one portion to a solution of the

above product (3.71 g, 17.3 mmol) in NaHCO₃ (5%, 100 mL) and dioxane (100 mL). After stirring for 3 h at room temperature, the solution was neutralized with 2 N HCl to pH 7. The reaction mixture was extracted with Et₂O (3 × 300 mL). The combined organic layers were dried (MgSO₄) and evaporated to give **7** (5.22 g, 96%) as a white solid. ¹H NMR (500 MHz, CDCl₃): δ = 1.26 (t, *J* = 7.0 Hz, 6H), 1.45 (s, 9H), 3.36 (m, 2H), 3.52 (m, 1H, 3H), 3.78 (m, 3H), 4.20 ppm (d, *J* = 7.1 Hz, 4H). ¹³C NMR (125 MHz, CDCl₃): δ = 13.1, 27.4, 44.3, 45.0, 46.9, 47.0, 60.3, 78.8, 152.8, 170.6 ppm. HRMS (EI) *m/z* C₁₅H₂₅NO₆ [MH⁺] calcd.: 315.1682; found: 315.1683.

rac-(3*S*,4*S*)-3,4-Bis-hydroxymethyl-pyrrolidine-1-carboxylic acid *tert*-butyl ester: LiBH₄ in THF (12 mL, 2 M, 24 mmol) was added dropwise to a solution of **7** (3.73 g, 11.8 mmol) in THF (100 mL) at 0 °C. The reaction mixture was allowed to reach room temperature and was stirred for a further 3 h. The solution was quenched with NaOH (200 mL, 1 N) and extracted with Et₂O (3 × 50 mL). The combined organic layers were dried (MgSO₄) and evaporated to give the diol (2.3 g, 84%) as a yellow solid. ¹H NMR (500 MHz, CDCl₃): δ = 1.45 (s, 9H), 2.22 (m, 1H), 3.74 (m, 4H), 3.93 ppm (m, 5H). ¹³C NMR (125 MHz, CDCl₃): δ = 28.6, 46.6, 48.4, 64.2, 79.6, 155.9 ppm. HRMS (EI) *m/z* C₁₁H₂₁NO₄ [MH⁺] calcd.: 231.1471; found: 231.1470.

rac-(3*S*,4*S*)-3-(*tert*-Butyl-dimethyl-silanyloxymethyl)-4-hydroxymethyl-pyrrolidine-1-carboxylic acid *tert*-butyl ester (**8**): The diol synthesized above (1.28 g, 5.5 mmol) was then dissolved in THF (100 mL), cooled to –10 °C, and treated with imidazole (360 mg, 5.5 mmol). After being stirred for 0.5 h, TBSCl (825 mg, 5.5 mmol) was added sequentially at –10 °C. The reaction mixture was added to a solution of water (100 mL) and brine (100 mL). The aqueous layer was extracted with Et₂O (3 × 50 mL), and the combined organic layers were washed with a solution of NaHSO₄ (10%, 2 × 100 mL), saturated NaHCO₃ (2 × 100 mL), and brine (2 × 100 mL). The product was dried (MgSO₄), filtered, and concentrated in vacuo. Flash chromatography (cyclohexane/EtOAc 1:1) furnished **8** (1.73 g, 90%) as a colorless oil. ¹H NMR (500 MHz, CDCl₃): δ = 0.01 (s, 6H), 0.81 (s, 9H), 1.36 (s, 9H), 2.08 (m, 2H), 2.91 (dd, *J* = 10.9, 8.7 Hz, 1H), 2.91 (m, 1H), 3.44 (dd, *J* = 10.3, 7.7 Hz, 1H), 3.47 ppm (m, 5H). ¹³C NMR (125 MHz, CDCl₃): δ = –5.4, 18.3, 25.9, 28.6, 45.2, 46.2, 48.4, 48.9, 64.1, 64.7, 79.3, 155.5 ppm. HRMS (ESI) *m/z* C₁₇H₃₅NO₄Si [MH⁺] calcd.: 346.2413; found: 346.2418. Anal. calcd. for C₁₇H₃₅NO₄Si: C 59.09, H 10.18, N 4.05; found: C 58.84, H 9.83, N 4.48.

rac-(3*S*,4*S*)-3-(*tert*-Butyl-dimethyl-silanyloxymethyl)-4-formyl-pyrrolidine-1-carboxylic acid *tert*-butyl ester (**9**): DMSO (0.84 g, 10.8 mmol, 3 equiv) was added dropwise to a solution of (COCl)₂ (0.68 g, 5.4 mmol, 1.5 equiv) in 50 mL CH₂Cl₂ at –78 °C under argon. The reaction mixture was stirred for 0.5 h with the dropwise addition of **8** (1.24 g, 3.6 mmol) dissolved in CH₂Cl₂ (50 mL). The reaction was maintained at –78 °C for 0.5 h followed by the addition of DIPEA (2.2 g, 21.6 mmol, 6 equiv). The reaction was allowed to warm to room temperature and was washed sequentially with HCl (1 N), saturated NaHCO₃, and brine solution. The organic layer was dried (MgSO₄), filtered, and concentrated in vacuo. Column chromatography (cyclohexane/EtOAc 1:1) of the residue provided **9**

(1.2 g, 98%) as a colorless oil. ^1H NMR (500 MHz, $[\text{D}_6]\text{DMSO}$): δ = 0.04 (s, 3H), 0.05 (s, 3H), 0.86 (s, 9H), 1.39 (s, 9H), 2.52 (m, 1H), 2.92 (m, 1H), 3.09 (m, 1H), 3.31 (m, 1H), 3.43 (m, 2H), 3.55 (m, 1H), 3.61 (m, 1H), 9.60 ppm (s, 1H). ^{13}C NMR (125 MHz, $[\text{D}_6]\text{DMSO}$): δ = -5.7, 17.7, 25.6, 27.9, 40.6, 44.4, 47.1, 52.0, 63.3, 78.3, 153.2, 201.7 ppm. Anal. calcd. for $\text{C}_{17}\text{H}_{33}\text{NO}_4\text{Si}$: C 59.37, H 9.60, N 4.07; found: C 59.06, H 9.30, N 3.66.

rac-(3*R*,4*S*)-3-((Benzyl-[2,6-dimethyl-phenoxy]-acetyl)-amino)-methyl-4-hydroxy-methyl-pyrrolidine-1-carboxylic acid tert-butyl ester (**10**): Benzylamine (280 mg, 3.6 mmol) was added to a solution of **9** (0.9 g, 2.6 mmol) in 100 mL THF at room temperature. The reaction mixture was then treated with orthoformate (380 mg, 2.6 mmol) and $\text{NMe}_4\text{BH}(\text{OAc})_3$ (950 mg, 3.6 mmol) at room temperature under N_2 for 12 h. The mixture was quenched by adding saturated NaHCO_3 (100 mL), and the product was extracted with EtOAc (3 \times 50 mL). The combined organic layers were extracted with HCl (1 N, 3 \times 100 mL) to transform the crude product into a HCl salt. The combined aqueous layers were saturated with K_2CO_3 and extracted with EtOAc (3 \times 100 mL). The combined organic layers were dried (MgSO_4), filtered, and concentrated in vacuo to give **10** (0.63 g, 75%) as a white solid. ^1H NMR (500 MHz, $[\text{D}_6]\text{DMSO}$): δ = 1.39 (s, 9H), 1.99 (m, 2H), 2.50 (m, 2H), 2.96 (m, 2H), 3.37 (m, 2H), 3.47 (m, 3H), 3.68 (m, 2H), 7.23 (m, 1H), 7.30 ppm (m, 4H). ^{13}C NMR (125 MHz, $[\text{D}_6]\text{DMSO}$): δ = 25.9, 39.5, 42.5, 46.1, 47.7, 48.5, 50.7, 59.9, 75.7, 124.3, 125.6, 125.7, 138.1, 151.2 ppm. Anal. calcd. for $\text{C}_{18}\text{H}_{28}\text{N}_2\text{O}_5$: C 67.41, H 8.74, N 8.74; found: C 67.20, H 8.50, N 8.77.

rac-(3*R*,4*S*)-3-((Benzyl-[2,6-dimethyl-phenoxy]-acetyl)-amino)-methyl-4-hydroxy-methyl-pyrrolidine-1-carboxylic acid tert-butyl ester: A solution of (2,6-dimethyl-phenoxy)acetic acid (240 mg, 1.3 mmol) and **10** (440 mg, 1.3 mmol) in anhydrous THF (100 mL) was cooled to 0 °C. Hydroxybenzotriazole (136 mg, 1.3 mmol) and EDC (260 mg, 1.3 mmol) were then added sequentially. The reaction mixture was stirred for 2 h at 0 °C, then warmed to 25 °C, and stirred for another 2 h. The organic layer was quenched with saturated NaHCO_3 and washed with brine solution. After extraction with Et_2O (3 \times 50 mL), the combined organic layers were dried with MgSO_4 , filtered, and evaporated in vacuo. The resulting material was subjected to flash silica gel chromatography, eluted with cyclohexane/EtOAc (1:1) to afford the product (510 mg, 77%) as a white solid. ^1H NMR (500 MHz, $[\text{D}_6]\text{DMSO}$): δ = 1.39 (s, 9H), 1.98 (m, 1H), 2.17 (m, 6H), 2.33 (m, 1H), 3.04 (m, 2H), 3.27 (m, 2H), 3.39 (m, 4H), 5.56 (m, 5H), 6.90 (m, 1H), 6.98 (m, 2H), 7.25 (m, 3H), 7.36 ppm (m, 2H). ^{13}C NMR (125 MHz, $[\text{D}_6]\text{DMSO}$): δ = 14.7, 28.8, 39.5, 44.7, 47.3, 50.1, 47.9, 48.4, 50.0, 50.4, 60.3, 71.0, 78.7, 124.6, 127.1, 127.6, 127.9, 128.1, 129.0, 129.3, 129.3, 129.3, 130.8, 137.8, 154.1, 156.2, 168.8 ppm. Anal. calcd. for $\text{C}_{28}\text{H}_{38}\text{N}_2\text{O}_5$: C 67.68, H 7.94, N 5.80; found: C 67.65, H 7.62, N 5.78.

rac-(3*R*,4*S*)-3-((Benzyl-[2,6-dimethyl-phenoxy]-acetyl)-amino)-methyl-4-formyl-pyrrolidine-1-carboxylic acid tert-butyl ester (**11**): Oxidation of the alcohol described above (310 mg, 0.64 mmol) with $(\text{COCl})_2$ (120 mg, 1 mmol, 1.5 equiv), DMSO (156 mg, 2 mmol, 3 equiv) and diisopropylamine (390 mg, 3.8 mmol, 6 equiv) as described for **9** was used to prepare **11** (170 mg) in 98% yield as a white solid. ^1H NMR (500 MHz, CDCl_3): δ = 1.45 (s, 9H), 2.24 (s, 6H), 2.91 (m, 2H), 3.09 (m, 1H), 3.28 (m, 1H),

3.46 (m, 4H), 4.59 (m, 4H), 6.91 (dd, J = 6.5, 5.6 Hz, 1H), 6.98 (d, J = 5.8 Hz, 2H), 7.20 (m, 2H), 7.34 (m, 3H), 9.65 ppm (s, 1H). ^{13}C NMR (125 MHz, $[\text{D}_6]\text{DMSO}$): δ = 15.9, 28.1, 37.4, 44.1, 46.9, 47.7, 49.8, 51.9, 70.1, 78.8, 123.9, 126.4, 127.0, 127.3, 127.5, 128.3, 128.6, 128.6, 128.6, 130.2, 137.3, 153.3, 155.4, 168.4, 201.6 ppm. Anal. calcd. for $\text{C}_{28}\text{H}_{36}\text{N}_2\text{O}_5$: C 69.98, H 7.55, N 5.83; found: C 69.86, H 7.38, N 6.15.

rac-(3*R*,4*R*)-3-((Benzyl-[2,6-dimethyl-phenoxy]-acetyl)-amino)-methyl-4-(isobutyl amino-methyl)-pyrrolidine-1-carboxylic acid tert-butyl ester (**12**): Reductive amination of **11** (210 mg, 0.43 mmol) with isobutylamine (31 mg, 0.43 mmol), orthoformate (63 mg, 0.43 mmol) and $\text{Me}_4\text{NBH}(\text{OAc})_3$ (158 mg, 0.60 mmol) described for **10** was used to prepare **12** (170 mg) in 75% yield as a white solid, which precipitated as hydrochloride from the aqueous phase. ^1H NMR (500 MHz, $[\text{D}_6]\text{DMSO}$): δ = 0.82 (s, 6H), 1.39 (s, 9H), 1.60 (m, 1H), 2.23 (m, 8H), 2.36 (m, 2H), 3.03 (m, 2H), 3.39 (m, 9H), 4.59 (m, 4H), 6.96 (m, 1H), 6.98 (m, 2H), 7.32 ppm (m, 5H). ^{13}C NMR (125 MHz, $[\text{D}_6]\text{DMSO}$): δ = 13.9, 15.9, 20.5, 27.7, 28.1, 39.5, 39.6, 47.3, 49.3, 49.4, 49.8, 51.5, 57.5, 70.4, 78.1, 123.9, 126.6, 127.0, 127.3, 127.5, 128.3 ppm. HRMS (ESI) m/z $\text{C}_{32}\text{H}_{47}\text{N}_3\text{O}_4$ $[\text{MH}^+]$ calcd.: 537.3567; found: 537.3571. Anal. calcd. for $\text{C}_{32}\text{H}_{47}\text{N}_3\text{O}_4\cdot\text{HCl}$: C 66.91, H 8.36, N 7.32; found: C 66.82, H 8.32, N 7.64.

rac-(3*S*,4*R*)-3-((Benzenesulfonyl-isobutyl-amino)-methyl)-4-((benzyl-[2-(2,6-dimethyl-phenoxy)-acetyl]-amino)-methyl)-pyrrolidine-1-carboxylic acid tert-butyl ester: TEA (24 mg, 0.23 mmol) and benzenesulfonyl chloride (42 mg, 0.24 mmol) were added to a solution of **12** (130 mg, 0.23 mmol) in 50 mL THF at 0 °C. After stirring for 2 h at room temperature, the reaction mixture was filtered and washed with brine (3 \times 50 mL). The organic layer was dried (MgSO_4), filtered, and evaporated under decreased pressure. Flash chromatography (EtOAc/MeOH 10:1) afforded the product (140 mg, 85%) as a white solid. ^1H NMR (500 MHz, $[\text{D}_6]\text{DMSO}$): δ = 0.80 (s, 6H), 1.39 (s, 9H), 1.82 (m, 1H), 2.14 (m, 8H), 2.77 (m, 3H), 3.07 (m, 2H), 3.32 (m, 5H), 4.61 (m, 4H), 6.90 (m, 1H), 6.98 (m, 2H), 7.32 (m, 5H), 7.58 (m, 2H), 7.77 ppm (m, 3H). ^{13}C NMR (125 MHz, $[\text{D}_6]\text{DMSO}$): δ = 13.9, 15.9, 19.8, 20.6, 26.6, 28.0, 39.5, 39.6, 47.0, 48.5, 48.6, 49.6, 51.4, 56.8, 70.2, 78.1, 123.9, 126.4, 126.9, 126.9, 127.0, 127.3, 127.6, 128.3, 128.6, 128.6, 130.1, 130.2, 132.7, 138.4, 145.3, 153.4, 156.6, 168.7 ppm. Anal. calcd. for $\text{C}_{38}\text{H}_{51}\text{N}_3\text{O}_6\text{S}$: C 67.33, H 7.58, N 6.20; found: C 67.22, H 7.55, N 6.32.

rac-(3*S*,4*S*)-N-[4-((Benzenesulfonyl-isobutyl-amino)-methyl)-pyrrolidine-3-ylmethyl]-N-benzyl-2-(2,6-dimethyl-phenoxy)-acetamide (**13**): HCl (20 mL, 4 N) in dioxane was added to a solution of the above-described product (100 mg, 0.14 mmol) in THF (40 mL) at room temperature. After stirring for 0.5 h the reaction mixture was evaporated under decreased pressure to give **13** (90 mg, quant.) as a white solid HCl salt. ^1H NMR (500 MHz, $[\text{D}_6]\text{DMSO}$): δ = 0.80 (s, 6H), 1.82 (m, 1H), 2.14 (s, 6H), 2.21 (m, 2H), 2.77–3.44 (m, 10H), 4.61 (m, 4H), 6.90 (m, 1H), 6.98 (m, 2H), 7.32 (m, 5H), 7.58 (m, 2H), 7.77 ppm (m, 3H). ^{13}C NMR (125 MHz, $[\text{D}_6]\text{DMSO}$): δ = 15.7, 19.7, 21.9, 26.7, 41.4, 42.2, 47.2, 48.2, 49.6, 50.0, 52.4, 56.5, 70.1, 123.8, 126.3, 126.9, 126.9, 127.1, 127.3, 127.5, 128.3, 128.6, 128.6, 130.1, 130.2, 132.6, 137.4, 138.7, 155.3, 167.9 ppm. HRMS (ESI) m/z $\text{C}_{33}\text{H}_{43}\text{N}_3\text{O}_4\text{S}$ $[\text{MH}^+]$ calcd.: 577.2955; found: 577.2974. Anal. calcd. for

(C₃₃H₄₃N₃O₄S·HCl)·H₂O: C 62.68, H 7.28, N 6.64; found: C 62.98, H 7.12, N 6.09.

rac-(3*S*,4*R*)-3-((Benzyl-[2-(2,6-dimethyl-phenoxy)-acetyl]-amino)-methyl)-4-[[isobutyl-(4-nitro-benzenesulfonyl)-amino]-methyl]-pyrrolidine-1-carboxylic acid *tert*-butyl ester was prepared in the same manner as described for the precursor of **13** by coupling 4-nitro-benzenesulfonyl chloride with **12** (53 mg, 0.24 mmol) to give the product (136 mg, 80%) as a white solid. ¹H NMR (500 MHz, [D₆]DMSO): δ = 0.80 (s, 6H), 1.39 (s, 9H), 1.82 (m, 1H), 2.14 (m, 8H), 2.77 (m, 3H), 3.07 (m, 2H), 3.32 (m, 5H), 4.61 (m, 4H), 6.90 (m, 1H), 6.98 (m, 2H), 7.26 (m, 5H), 8.09 (d, *J* = 7.9 Hz, 2H), 8.40 ppm (d, *J* = 6.9 Hz, 2H). ¹³C NMR (125 MHz, [D₆]DMSO): δ = 13.9, 15.8, 19.6, 20.6, 26.6, 28.0, 39.5, 39.6, 47.2, 48.6, 49.7, 51.4, 56.5, 59.6, 70.1, 78.1, 123.9, 124.4, 124.4, 126.3, 127.0, 127.3, 127.5, 128.3, 128.6, 128.6, 130.1, 136.9, 137.2, 144.0, 149.7, 153.4, 155.2, 168.2, 170.1 ppm. HRMS (ESI) *m/z* C₃₈H₅₁N₄O₈S [MH⁺] calcd.: 723.3416; found: 723.3427.

rac-(3*S*,4*S*)-*N*-{4-[[[(4-Amino-benzenesulfonyl-isobutyl-amino)-methyl]-pyrrolidin-3-ylmethyl]-*N*-benzyl-2-(2,6-dimethyl-phenoxy)-acetamide (**14**) was prepared in the same fashion as **13** by the addition of SnCl₂ (50 mg, 0.28 mmol) to give **14** (92 mg, quant.) as a white HCl salt. ¹H NMR (500 MHz, [D₆]DMSO): δ = 0.80 (s, 6H), 1.85 (m, 1H), 2.17 (s, 8H), 2.70 (m, 7H), 3.31 (m, 6H), 4.51 (m, 4H), 5.96 (s, 2H), 6.64 (d, *J* = 8.8 Hz, 2H), 6.90 (m, 1H), 6.98 (m, 2H), 7.32 ppm (m, 5H). ¹³C NMR (125 MHz, [D₆]DMSO): δ = 15.7, 19.7, 22.5, 26.8, 41.5, 41.9, 47.2, 48.4, 48.6, 50.2, 52.7, 56.8, 70.1, 112.6, 123.8, 126.3, 126.9, 127.1, 127.5, 128.3, 128.6, 128.6, 128.8, 130.1, 132.6, 137.4, 152.6, 167.9 ppm. HRMS (ESI) *m/z* C₃₃H₄₄N₄O₄S [MH⁺] calcd.: 592.3083; found: 592.3053. Anal. calcd. for C₃₃H₄₃N₄O₄S·HCl: C 63.05, H 7.15, N 8.90; found: C 63.46, H 7.15, N 8.52.

rac-(3*S*,4*R*)-3-((Benzyl-[2-(2,6-dimethyl-phenoxy)-acetyl]-amino)-methyl)-4-[[isobutyl-(4-toluene-4-sulfonyl)-amino]-methyl]-pyrrolidine-1-carboxylic acid *tert*-butyl ester was prepared in the same manner as described for the precursor of **13** by coupling 4-methyl-benzenesulfonyl chloride with **12** (45 mg, 0.24 mmol) to give the product (128 mg, 81%) as a white solid. ¹H NMR (500 MHz, [D₆]DMSO): δ = 0.80 (s, 6H), 1.39 (s, 9H), 1.82 (m, 1H), 2.14 (m, 7H), 2.50 (s, 3H), 2.77 (m, 3H), 3.07 (m, 3H), 3.32 (m, 5H), 4.44 (m, 4H), 6.90 (m, 1H), 6.98 (m, 2H), 7.26 (m, 5H), 7.39 (d, *J* = 8.0 Hz, 2H), 7.66 ppm (d, *J* = 7.4 Hz, 2H). ¹³C NMR (125 MHz, [D₆]DMSO): δ = 15.7, 19.7, 20.8, 26.7, 28.0, 39.5, 39.6, 47.2, 48.6, 49.6, 51.6, 56.9, 70.1, 78.1, 123.9, 126.3, 126.6, 126.6, 127.2, 127.5, 128.3, 128.6, 128.6, 130.1, 135.4, 136.9, 143.0, 153.3, 155.3, 168.2 ppm. Anal. calcd. for C₃₉H₅₃N₃O₆S: C 67.70, H 7.72, N 6.07; found: C 67.99, H 7.69, N 6.31.

rac-(3*S*,4*S*)-*N*-Benzyl-2-(2,6-dimethyl-phenoxy)-*N*-4-[[isobutyl-(toluene-4-sulfonyl)-amino]-methyl]-pyrrolidin-3-ylmethyl)-acetamide (**15**) was prepared in the same fashion as **13** to give the product (93 mg, quant.) as a white HCl salt. ¹H NMR (500 MHz, [D₆]DMSO): δ = 0.80 (s, 6H), 1.85 (m, 1H), 2.17 (s, 8H), 2.49 (s, 3H), 2.84 (m, 5H), 3.31 (m, 6H), 4.51 (m, 4H), 6.90 (m, 1H), 6.98 (m, 2H), 7.32 (m, 7H), 7.65 ppm (m, 2H). ¹³C NMR (125 MHz, [D₆]DMSO): δ = 15.7, 19.7, 20.8, 26.7, 41.5, 41.9, 47.2, 48.2, 49.6, 50.3, 52.7, 56.6, 70.1, 123.8, 126.3, 126.9, 126.9, 127.2, 127.5, 128.3, 128.6, 128.6, 129.6, 129.6, 130.1, 130.2, 135.7, 137.1, 142.9, 152.6, 167.7 ppm. HRMS (ESI) *m/z* C₃₄H₄₅N₃O₄S [MH⁺]

calcd.: 591.3131; found: 591.3111. Anal. calcd. for C₃₄H₄₅N₃O₄S·HCl: C 64.93, H 7.32, N 6.68; found: C 65.19, H 7.61, N 6.34.

Acknowledgments

The authors are grateful to Bayer AG, Wuppertal, Germany for financial support. The clone of the protease was kindly provided by Professor Helena Danielson, University of Uppsala, Department of Biochemistry, Uppsala, Sweden. We acknowledge the support of the beamline staff at BESSY II, Berlin, Germany.

Keywords: antiviral agents • enzymes • inhibitors • proteases • pyrrolidines

- [1] D. Leung, G. Abbenante, D. P. Fairlie, *J. Med. Chem.* **2000**, *43*, 305–340.
- [2] D. H. Rich, *J. Med. Chem.* **1985**, *28*, 263–273.
- [3] C. A. Lipinski, F. Lombardo, B. W. Dominy, P. J. Feeney, *Adv. Drug Delivery Rev.* **1997**, *23*, 3–25.
- [4] a) M. A. Navia, P. M. Fitzgerald, B. M. McKeever, C. T. Leu, J. C. Heimbach, W. K. Herber, I. S. Sigal, P. L. Darke, J. P. Springer, *Nature* **1989**, *337*, 615–620; b) A. Wlodawer, M. Miller, M. Jaskolski, B. K. Sathyanarayana, E. Baldwin, I. T. Weber, L. M. Selk, L. Clawson, J. Schneider, S. B. Kent, *Science* **1989**, *245*, 616–621.
- [5] D. Askin, *Curr. Opin. Drug Discovery Dev.* **1998**, *1*, 338–348.
- [6] F. E. Boyer, J. V. Vara Prasad, J. M. Domatola, E. L. Ellsworth, C. Gajda, S. E. Hagen, L. J. Markoski, B. D. Tait, E. A. Lunney, A. Palovsky, D. Ferguson, N. Graham, T. Holler, D. Hupe, C. Nouhan, P. J. Tummino, A. Urumov, E. Zeikus, G. Zeikus, S. J. Gracheck, J. M. Sanders, S. VanderRoest, J. Brod-fuehrer, K. Iyer, M. Sinz, S. V. Gulnik, J. W. Erickson, *J. Med. Chem.* **2000**, *43*, 843–858.
- [7] M. G. Bursavich, D. H. Rich, *J. Med. Chem.* **2002**, *45*, 541–558.
- [8] L. Romano, G. Venturi, S. Giomi, L. Pippi, P. E. Valensin, M. Zazzi, *J. Med. Virol.* **2002**, *66*, 143–150.
- [9] S. Thaisrivongs, J. W. Strohbach, *Biopolymers* **1999**, *51*, 51–58.
- [10] E. Vieira, A. Binggeli, V. Breu, D. Bur, W. Fischli, R. Güller, G. Hirth, H. P. Märki, M. Müller, C. Oefner, M. Scalone, H. Stadler, M. Wilhelm, W. Wostl, *Bioorg. Med. Chem. Lett.* **1999**, *9*, 1397–1402.
- [11] R. Güller, A. Binggeli, V. Breu, D. Bur, W. Fischli, G. Hirth, C. Jenny, M. Kansy, F. Montavon, M. Müller, C. Oefner, H. Stadler, E. Vieira, M. Wilhelm, W. Wostl, H. P. Märki, *Bioorg. Med. Chem. Lett.* **1999**, *9*, 1403–1408.
- [12] H. Ohtaka, A. Schön, E. Freire, *Biochemistry* **2003**, *42*, 13659–13666.
- [13] L. Prade, A. F. Jones, C. Boss, S. Richard-Blichstein, S. Meyer, C. Binkert, D. Bur, *J. Biol. Chem.* **2005**, *280*, 23837–23843.
- [14] P. M. D. Fitzgerald, B. M. McKeever, J. F. VanMiddlesworth, J. P. Springer, J. C. Heimbach, C.-T. Leu, W. K. Herber, R. A. F. Dixon, P. L. Darke, *J. Biol. Chem.* **1990**, *265*, 14209–14219.
- [15] E. T. Baldwin, T. N. Bhat, S. Gulnik, M. V. Hosur, D. Sowder, R. E. Cachau, J. Collins, A. M. Silva, J. W. Erickson, *Proc. Natl. Acad. Sci. USA* **1993**, *90*, 6796–6799.
- [16] E. E. Kim, C. T. Baker, M. D. Dwyer, M. A. Murcko, B. G. Rao, R. D. Tung, M. A. Navia, *J. Am. Chem. Soc.* **1995**, *117*, 1181–1182.
- [17] E. C. Lee, E. K. Kick, J. A. Ellman, *J. Am. Chem. Soc.* **1998**, *120*, 9735–9747.
- [18] J. Mancuso, D. S. Brownfain, D. Swern, *J. Org. Chem.* **1979**, *44*, 4148–4150.
- [19] A. F. Abdel-Magid, K. G. Carson, B. D. Harris, C. A. Maryanoff, R. D. Shah, *J. Org. Chem.* **1996**, *61*, 3849–3862.
- [20] G. Müller, C. Kallus, A. Schoop, *unpublished results*.
- [21] M. V. Toth, G. R. Marshall, *Int. J. Pept. Protein Res.* **1990**, *36*, 544–550.
- [22] S. V. Gulnik, L. I. Suvarov, P. Majer, J. Collins, P. K. Bradley, D. G. Johnson, J. W. Erickson, *FEBS Lett.* **1997**, *413*, 379–384.
- [23] H. Gohlke, M. Hendlich, G. Klebe, *J. Mol. Biol.* **2000**, *295*, 337–356.
- [24] D. S. Goodsell, G. M. Morris, A. J. Olson, *J. Mol. Recognit.* **1996**, *9*, 1–5.
- [25] G. M. Morris, D. S. Goodsell, R. S. Halliday, R. Huey, W. E. Hart, R. K. Belew, A. J. Olson, *J. Comput. Chem.* **1998**, *19*, 1639–1662.

- [26] C. A. Sotriffer, H. Gohlke, G. Klebe, *J. Med. Chem.* **2002**, *45*, 1967–1970.
- [27] S. Schmitt, D. Kuhn, G. Klebe, *J. Mol. Biol.* **2002**, *323*, 387–406.
- [28] S. Schmitt, M. Hendlich, G. Klebe, *Angew. Chem.* **2001**, *113*, 3237–3241; *Angew. Chem. Int. Ed.* **2001**, *40*, 3141–3144.
- [29] E. Specker, J. Böttcher, H. Lilie, A. Heine, A. Schoop, G. Müller, N. Griebel, G. Klebe, *Angew. Chem.* **2005**, *117*, 3200–3204; *Angew. Chem. Int. Ed.* **2005**, *44*, 3140–3144.
- [30] A. Taylor, D. P. Brown, S. Kadam, M. Maus, W. E. Kohlbrenner, D. Weigl, M. Turon, L. Katz, *Appl. Microbiol. Biotechnol.* **1992**, *37*, 205–210.
- [31] Z. Otwinowski, W. Minor, *Methods Enzymol.* **1997**, *276A*, 307–326.
- [32] J. Navaza, *Acta Crystallogr. Sect. A* **1994**, *50*, 157–163.
- [33] J. L. Martin, J. Begun, A. Schindeler, W. A. Wickramasinghe, D. Alewood, P. F. Alewood, D. A. Bergmann, R. I. Brinkworth, G. Abbenante, D. R. March, R. C. Reid, D. P. Fairlie, *Biochemistry* **1999**, *38*, 7978–7988.
- [34] G. M. Sheldrick, T. R. Schneider, *Methods Enzymol.* **1997**, *277A*, 319–343.
- [35] T. A. Jones, J. Y. Zou, S. W. Cowan, M. Kjeldgaard, *Acta Crystallogr. Sect. A* **1991**, *47*, 110–119.
- [36] K. Bäckbro, S. Löwgren, K. Österlund, J. Atepo, T. Unge, J. Hultén, N. M. Bonham, W. Schaal, A. Karlén, A. Hallberg, *J. Med. Chem.* **1997**, *40*, 898–902.
- [37] N. M. King, L. Melnick, M. Prabu-Jeyabalan, E. A. Nalivaika, S. S. Yang, Y. Gao, X. Nie, C. Zepp, D. L. Heefner, C. A. Schiffer, *Protein Sci.* **2002**, *11*, 418–429.
- [38] G. Abbenante, D. R. March, D. A. Bergman, P. A. Hunt, B. Garnham, R. J. Dancer, J. L. Martin, D. P. Fairlie, *J. Am. Chem. Soc.* **1995**, *117*, 10220–10226.
- [39] Z. Chen, Y. Li, E. Chen, D. L. Hall, P. L. Darke, C. Culberson, J. A. Shafer, L. C. Kuo, *J. Biol. Chem.* **1994**, *269*, 26344–26348.
- [40] R. B. Rose, C. S. Craik, N. L. Douglas, R. M. Stroud, *Biochemistry* **1996**, *35*, 12933–12944.
- [41] R. March, G. Abbenante, D. A. Bergman, R. I. Brinkworth, W. Wickramasinghe, J. Begun, J. L. Martin, D. P. Fairlie, *J. Am. Chem. Soc.* **1996**, *118*, 3375–3379.
- [42] B. M. Mahalingam, J. Louis, C. C. Reed, J. M. Adomat, J. Krouse, Y. F. Wang, R. Harrison, I. T. Weber, *Eur. J. Biochem.* **1999**, *263*, 238–245.
- [43] W. Schaal, A. Karlsson, G. Ahlsén, J. Lindberg, H. O. Andersson, U. H. Danielson, B. Classon, T. Unge, B. Samuelsson, J. Hultén, A. Hallberg, A. Karlén, *J. Med. Chem.* **2001**, *44*, 155–169.
- [44] R. Bone, J. P. Vacca, P. S. Anderson, M. K. Holloway, *J. Am. Chem. Soc.* **1991**, *113*, 9382–9384.
- [45] B. M. Mahalingam, J. M. Louis, J. Hung, R. W. Harrison, I. T. Weber, *Proteins Struct. Funct. Genet.* **2001**, *43*, 455–464.
- [46] S. Munshi, Z. Chen, Y. Li, D. B. Olsen, M. E. Fraley, R. W. Hungate, L. C. Kuo, *Acta Crystallogr. Sect. D* **1998**, *54*, 1053–1060.
- [47] M. Miller, J. Schneider, B. K. Sathyanarayana, M. V. Toth, G. R. Marshall, L. Clawson, L. Selk, K. B. Kent, A. Wlodawer, *Science* **1989**, *246*, 1149–1152.
- [48] M. V. Hosur, T. N. Bhat, D. J. Kempf, E. T. Baldwin, B. S. Liu, S. Gulnik, N. E. Wideburg, D. W. Norbeck, K. Appelt, J. W. Erickson, *J. Am. Chem. Soc.* **1994**, *116*, 847–855.

Received: July 11, 2005

Revised: October 19, 2005

Published online on December 5, 2005